



1 **Modeling 21st century snow dynamics in Switzerland using** 2 **high-resolution Climate CH2025 scenarios**

3 Harsh Beria^{1,2,3}, Sven Kotlarski^{2,4}, Adrien Michel², Jan Magnusson¹, Christoph Marty¹

4 ¹ WSL Institute for Snow and Avalanche Research SLF, Davos, Switzerland

5 ² Federal Office of Meteorology and Climatology, MeteoSwiss, Zurich, Switzerland

6 ³ Department of Civil, Environmental and Geomatic Engineering, ETH Zurich, Zurich, Switzerland

7 ⁴ Center for Climate Systems Modeling C2SM, ETH Zurich, Zurich, Switzerland

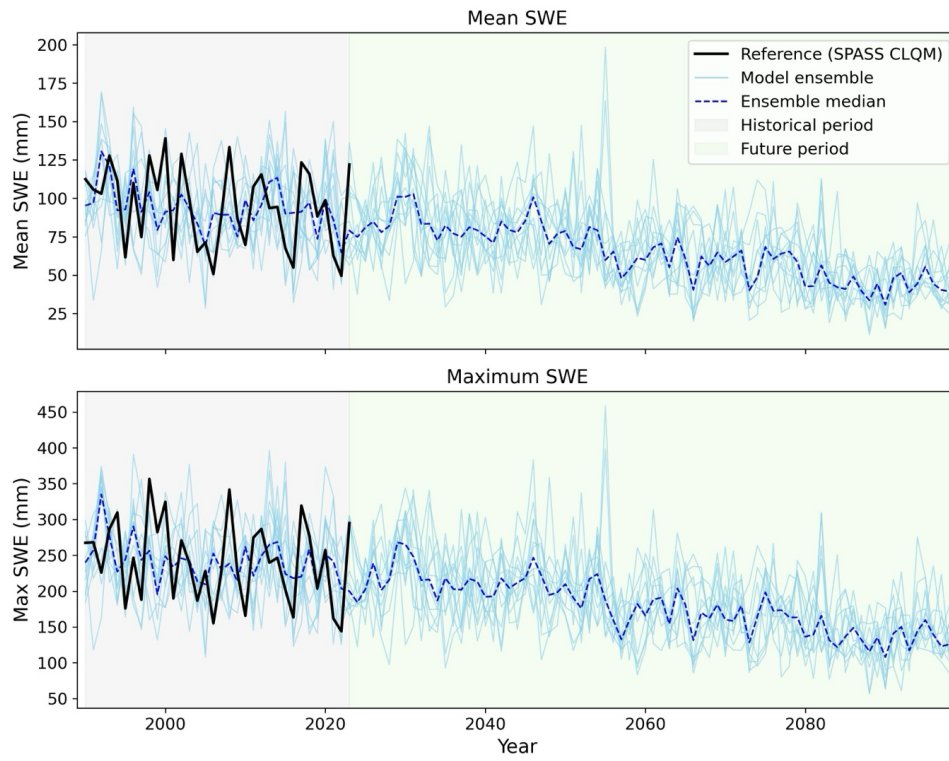
8 *Correspondence to:* Harsh Beria (hberia@ethz.ch)

9 **Abstract.** Snow is a key component of Alpine landscapes, providing numerous ecosystem and economic services
10 that include hydropower production, winter tourism, groundwater recharge, and regulation of stream temperatures,
11 with significant implications for aquatic ecosystems. In a warming climate, expected increases in winter
12 precipitation do not necessarily lead to greater snow accumulation, as rising air temperatures shift precipitation
13 from snowfall to rainfall and reduce the persistence of snow on the ground. This creates a need for future snow
14 projections at locally relevant spatial scales to support adaptation for snow-dependent sectors.

15 Here, we present daily projections of snow water equivalent (SWE) for Switzerland at 1x1 km² resolution, based
16 on the Climate CH2025 scenarios, which downscaled and bias-adjusted meteorological forcings from an ensemble
17 of EURO-CORDEX regional climate models. SWE was simulated using a spatially distributed temperature-index
18 snow model for 12 climate model chains, selected for their ability to accurately represent atmospheric forcings
19 for modeling snow cover dynamics across Switzerland over the historical reference period (1991-2020). To reduce
20 biases associated with the simplified degree-day-based snowmelt representation used here, simulated SWE was
21 quantile mapped toward SPASS-CLQM, a new gridded climatological snow reference dataset for Switzerland.

22 We found that the univariate quantile mapping of meteorological forcings in Climate CH2025 models reduced
23 precipitation under sub-freezing conditions, resulting in too little simulated snowfall in many model chains, which
24 then propagated nearly linearly into biases in SWE. Simulated SWE in the final set of 12 models was additionally
25 quantile mapped toward SPASS-CLQM, which substantially reduced SWE biases across elevation bands and was
26 then applied to future simulations. By the end of century (2069-2099), projected SWE showed widespread
27 declines across Switzerland relative to 1991-2020. Percentage September-May mean SWE losses exceeded 80%
28 below 1000 m a.s.l. for the highest emission pathway (RCP8.5), where snow became increasingly rare. At
29 intermediate elevations (1000-2000 m a.s.l.), mean SWE declines of 50-90% are projected, with the snowpack
30 becoming increasingly ephemeral. Above 2000 m a.s.l., mean SWE reductions ranged from 20 to 70%, indicating
31 that even high-elevation seasonal snow storage would reduce substantially. These projections provide a spatially
32 detailed basis for assessing future changes in Alpine snow resources and for informing the management of snow-
33 dependent hydrological, ecological, and economic systems in a rapidly warming climate.

34 **Keywords:** snow; alpine hydrology; Switzerland; climate scenarios



35

36



37 **1 Introduction**

38 Snow is a central component of the Alpine hydrological cycle, with seasonal snowpacks storing winter
39 precipitation and releasing this water during spring and early summer, thereby shaping the timing of peak runoff,
40 modulating groundwater recharge through snowmelt pathways (Beria et al., 2020), regulating stream water
41 temperature (van Hamel and Brunner, 2024; Michel et al., 2020) and sustaining summer low flows (Jenicek et al.,
42 2016). Apart from these ecosystem services, snow has important economic roles in diverse sectors including in
43 hydropower generation (Schaepli, 2015) and in winter tourism (Morin et al., 2021; Willibald et al., 2021).
44 Snowpack also modulates natural hazards such as snowmelt-induced floods and avalanches (Beniston et al., 2007;
45 Harpold et al., 2017; Mayer et al., 2024). In large parts of Switzerland, winter temperatures used to stay below
46 0°C for sustained periods, but in the last decades, increasing air temperature reduces snow accumulation (Serquet
47 et al., 2011) and advances the timing of snowmelt, thereby reducing persistence of snowpack (Klein et al., 2016).
48 This makes snow on the ground an important barometer of the effects of climate change and a key variable for
49 climate-impact assessments in complex mountain landscapes.

50 Existing snow depth measurements across the European Alps have shown significant reductions in snow
51 accumulation over recent decades. An Alpine-wide analysis of snow depth records showed widespread declines
52 in snow depth and seasonal snow cover duration from 1971 to 2019, with mean and maximum November-May
53 snow depth decreasing by 8.4% and 5.6% per decade respectively, and snow cover duration shortening by 5.6%
54 per decade (Matiu et al., 2021). Recent model-based snow reanalysis has shown elevation-dependent reductions
55 in snow depth, with the lower elevation (< 1000 m a.s.l.) Swiss plateau witnessing larger decreases in snow depth
56 of 10-20% per decade, and snow depth above 1000 m a.s.l. showing losses of 5-10% per decade (Marty et al.,
57 2025). Longer-term reconstructions based on shrub ring-width from the Italian Alps indicate that current
58 snowpack duration at about 2000 m is approximately 36 days shorter than the long-term mean of the last six
59 centuries (Carrer et al., 2023), suggesting an unprecedented decline on centennial timescales. Snow depth
60 measurements from Austria and Switzerland reveal that between 1961 and 2012 snowpack duration decreased by
61 about 24 days at 1500 m (Schöner et al., 2019).

62 Similar declining patterns have been seen in snow water equivalent (SWE), which is directly linked to seasonal
63 meltwater fluxes. An analysis of long-term SWE measurements in five Alpine countries revealed systematic
64 reduction in SWE across locations, independent of the latitude or longitude of the site, with more pronounced
65 SWE reduction seen during spring relative to winter (Marty et al., 2017b). SWE in the Italian and the Swiss Alps
66 has also seen significant decreases in recent decades (Dall'Amico et al., 2025; Marty et al., 2025; Ranzi et al.,
67 2024), with largest SWE losses at the tail of the snow season (Colombo et al., 2022). Together, these studies show
68 that both snow depth and SWE are declining substantially across the Alps.

69 Future snow projections indicate a continuation and amplification of these changes. Regional climate simulations
70 over the European Alps project seasonal redistribution of precipitation from summer toward winter (Frei et al.,
71 2018; Lüthi et al., 2019, Kotlarski et al., 2023). Despite projected increases in winter precipitation, mean
72 September-May snowfall is expected to reduce by 25% and 45% for the RCP 4.5 and 8.5 greenhouse gas scenarios,
73 respectively, until 2100, with snowfall reduction exceeding 80% in lower elevation (<1000 m a.s.l.) alpine regions
74 (Frei et al., 2018). Under the high-emission scenario RCP8.5, SWE reduction until the end of 21st century is



75 expected to follow an elevation-dependent pattern, with lower elevation regions showing larger relative SWE
76 reductions exceeding 80%. Even at higher elevations (>2500 m a.s.l.), SWE is projected to reduce between 30-
77 50% (Kotlarski et al., 2023).

78 Alongside lower SWE, Alpine snowpacks are projected to melt earlier, with snowmelt dates expected to advance
79 at a rate of 6 days per decade under the RCP8.5 scenario (Vorkauf et al., 2021). Continuous snow cover is likely
80 to become restricted to elevations above 2000 m a.s.l., while mid-elevation snowpacks (1000-1700 m a.s.l.)
81 become increasingly ephemeral (Schmucki et al., 2017). These projected changes arise from the combined effects
82 of reduced snowfall, shorter accumulation seasons, earlier melt, with increases in winter precipitation only partly
83 compensating for warming with its effects being limited to very high elevation regions, which remain poorly
84 resolved in existing climate models (Kotlarski et al., 2023; Lüthi et al., 2019).

85 For assessing future snow cover evolution, a straightforward approach is to analyze snow cover characteristics as
86 simulated by the land surface schemes of global or regional climate models. Global climate models provide
87 physically consistent large-scale climate projections but are too coarse to accurately represent the complex Alpine
88 topography. Dynamical downscaling using an ensemble of regional climate models, such as the EURO-CORDEX,
89 preserves the physical relationships between the different meteorological variables. However, such models still
90 poorly resolve surface topography with coarse grid spacings of ~12 km, which smoothens elevation, slope, and
91 valley curvatures in steep terrain. Kilometer-scale convection-permitting models have emerged as a potential
92 solution with early studies showing added value for Alpine SWE simulations (Lüthi et al., 2019). However, these
93 remain computationally expensive and are available only for small time slices (e.g., 10-year periods). Recent
94 studies have also shown that fine-scale convection permitting models add value for summer convection and sub-
95 daily precipitation extremes, but their added value for winter precipitation is less clear, because winter
96 precipitation in the Alps is more strongly governed by large-scale circulation, than by local convective processes
97 (Estermann et al., 2025). Therefore, the added value of higher-resolution and computationally expensive
98 convection permitting models on snow accumulation and ablation remains unclear.

99 Another alternative for producing SWE projections at locally relevant spatial resolutions is by downscaling and
100 bias-adjusting meteorological outputs from regional climate models to higher resolutions at which the dominant
101 effects of topography can be accurately represented (Chen et al., 2013; Matiu and Hanzer, 2022; MeteoSwiss and
102 Zurich, 2025). Such climate forcings can then be used to simulate SWE using process-based snow models. Such
103 workflows provide detailed representation of snow accumulation and melt dynamics and have shown promising
104 results when applied at stations or over catchments (Marke et al., 2015; Marty et al., 2017a; Schmucki et al., 2015,
105 2017). A limitation of such approaches is that bias adjustment methods can affect inter-variable dependencies and
106 their spatial and temporal coherence, which is critical for snow applications because snowfall depends on the joint
107 distribution of precipitation and temperature (Astagneau et al., 2025; François et al., 2020; Matiu et al., 2024;
108 Michel et al., 2024). Despite these limitations, bias adjustment of dynamically downscaled climate models remains
109 one of the most relevant methods to estimate future changes in SWE at higher spatial resolutions. However, SWE
110 projections at national scale in the European Alps remain limited.

111 Several recent efforts have moved toward more spatially detailed Alpine snow projections. Matiu and Hanzer
112 (2022) downscaled and bias-adjusted snow cover fractions from EURO-CORDEX simulations using long-term



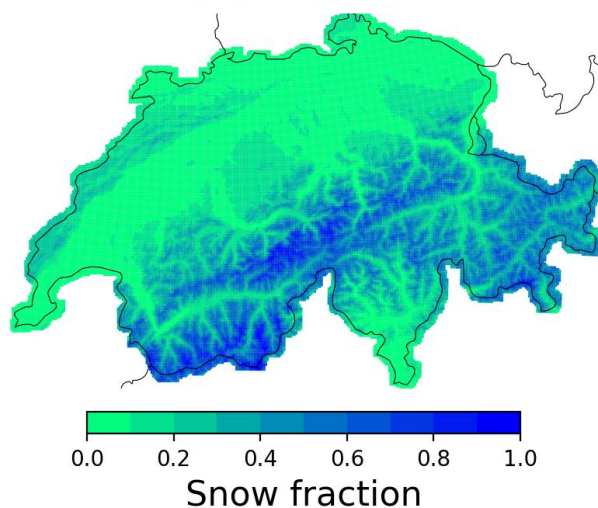
113 remote sensing observations across the greater Alpine domain. The Copernicus Climate Change Services provided
114 mountain tourism snow indicators for administrative regions in the European Alps based on bias-adjusted EURO-
115 CORDEX projections and the Crocus snow model (Morin et al., 2021), while national initiatives such as FuSE-
116 AT in Austria developed snow-related indicators based on the SNOWGRID model from their national climate
117 scenarios (Olefs et al., 2020). Similar initiatives are currently being undertaken in Italy within the IT-WATER
118 project. For Switzerland, a spatially continuous daily SWE projection dataset at high spatial resolution and
119 consistent with the national reference climate scenarios has so far been missing.

120 Here, we address this gap by producing daily SWE projections for Switzerland at 1×1 km² resolution using
121 meteorological forcings from a selected subset of models from the Climate CH2025 scenarios. These scenarios
122 provide statistically bias adjusted and downscaled daily meteorological fields for Switzerland, based on EURO-
123 CORDEX simulations (MeteoSwiss and Zurich, 2025). The objectives are to: (1) identify the model chains that
124 adequately represent historical snow conditions over the reference period (1991-2020), (2) develop a methodology
125 to simulate daily SWE with a spatially distributed snow model for the selected model chains, (3) improve the
126 simulated SWE by leveraging the recently developed SPASS reference snow climatology (Marty et al., 2025;
127 Michel et al., 2024), and (4) quantify projected changes in SWE across Switzerland until the end of the 21st
128 century. By linking the Climate CH2025 scenarios with a high-resolution, observation-constrained SWE reference
129 dataset, this study provides the first spatially explicit basis for assessing future changes in Swiss snow resources
130 and their hydrological, ecological, and socioeconomic implications.

131 **2 Study area and methods**

132 Switzerland experiences strong climatic and topographic gradients over a relatively small area. The European
133 Alps split Switzerland into two distinct climate zones: a continental climate in the North and a temperate
134 Mediterranean climate in the South. With some degree of simplification, the country can be divided into three
135 main physiographic regions: the Jura Mountains in the Northwest, the high-elevation Alps in the South, and the
136 Central Plateau in between (Figure 1), which respectively account for 10%, 30%, and 60% of the total land area
137 (Obuchowicz et al., 2023). Forest composition follows distinct elevational gradients, with deciduous beech forests
138 primarily occupying lower elevation regions in Jura and Swiss Plateau, and coniferous forests (primarily spruce
139 and larch) becoming more dominant in higher elevation subalpine regions (Wüest et al., 2020). Seasonal snowpack
140 is most persistent in the Alpine regions, where winter precipitation frequently falls as snow (Figure 1). In contrast,
141 the Swiss Plateau and lower elevation valleys in Northern Switzerland experience only intermittent snowfall
142 (Marty et al., 2025).

143



144

145 Figure 1: Snowfall fraction across Switzerland for the 1991-2020 reference period, calculated from daily 1x1 km²
146 observational precipitation and air temperature forcings based on RhiresD and TabsD datasets, respectively
147 (MeteoSwiss, 2016, 2017). The Swiss Plateau is the large green area between the Alps in the South and Jura in
148 Northwest. Snowfall fraction is defined as the proportion of total precipitation falling as snow, with snowfall
149 calculated using the precipitation-phase partitioning method from the operational snow-hydrological service
150 (OSHD; Mott et al., 2023; Magnusson et al., 2014).

151 2.1 Climate CH2025 scenarios

152 Climate CH2025 scenario is the fourth generation of national climate scenarios for Switzerland, following
153 CH2007, CH2011, and CH2018, providing the most recent assessment of past and future climate change in
154 Switzerland. Climate CH2025 scenarios combine long-term observational records, EURO-CORDEX regional
155 climate simulations, and CMIP6 global climate information (MeteoSwiss and Zurich, 2025). In contrast to earlier
156 Swiss climate scenarios, Climate CH2025 expresses future changes primarily in the frame of Global Warming
157 Levels, using a block-time-shift approach to link CMIP5-based EURO-CORDEX regional simulations with
158 CMIP6 global warming trajectories (MeteoSwiss and Zurich, 2025; Michel et al., 2024).

159 For climate impact applications, Climate CH2025 provides, among other variables, statistically bias-adjusted and
160 spatially downscaled daily gridded precipitation and air temperature fields at 1x1 km² resolution over Switzerland,
161 using univariate quantile mapping, with 1991-2020 set as the reference period. Climate CH2025 shows that
162 Switzerland is warming at more than twice the global rate, with future projections suggesting even drier summers,
163 increased precipitation extremes, and reduced snow cover. Detailed results from these scenarios are provided in
164 the Climate CH2025 scientific report (MeteoSwiss and Zurich, 2025).

165 2.2 Snow modeling

166 In the present study, SWE was simulated using a spatially distributed temperature-index snow model, driven by
167 atmospheric forcing from the bias-adjusted gridded CH2025 datasets. The snow model is part of the operational



168 snow-hydrological service (OSHD; Mott et al., 2023) of the WSL Institute for Snow and Avalanche Research
169 SLF and, in combination with a data assimilation procedure, is used to produce long-term SWE climatology for
170 Switzerland (Marty et al., 2025; Mott et al., 2023). Both the model and the data assimilation scheme are described
171 in Magnusson et al. (2014). The model requires only daily precipitation and air temperature as meteorological
172 forcings, and its main state variables are SWE and liquid water content. The degree-day factors vary seasonally
173 to reflect changes in day length. In addition, the model includes an algorithm for estimating the fraction of snow-
174 covered area (Magnusson et al., 2014; Mott et al., 2023).

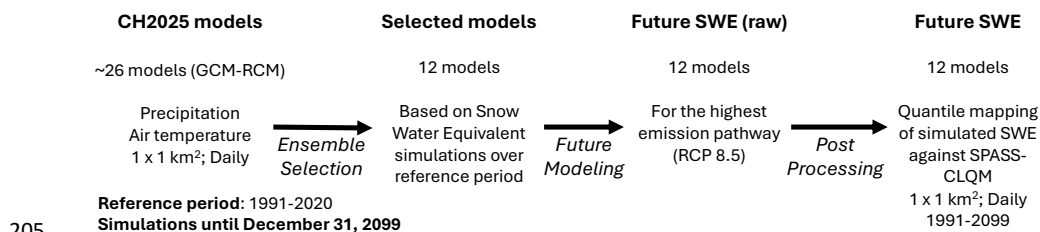
175 The model was run at a daily timestep and at 1x1 km² spatial resolution for individual hydrological years, defined
176 from 1 September to 31 August. Snow simulations were performed for both the observational reference forcings
177 (1991-2020), based on the gridded RhiresD and TabsD datasets (MeteoSwiss, 2016, 2017), and for each selected
178 Climate CH2025 model chain (for the RCP8.5 greenhouse gas scenario) covering the period 1991-2099. This
179 setup ensured that differences between historical reference simulations and climate-model-driven simulations
180 arose primarily from differences in meteorological forcings.

181 **2.3 Model sub-selection for future snow simulations and bias adjustment of SWE**

182 Climate CH2025 scenarios provide gridded precipitation and temperature forcings for an ensemble of 26 climate
183 models for different emission pathways. Before producing future snow projections, we evaluated the ability of
184 each model chain to represent snowfall and SWE over the 1991-2020 reference period. Snowfall was computed
185 using a continuous, temperature-dependent precipitation partitioning routine, similar to the approach used in
186 OSHD (Magnusson et al., 2014). For each model chain, annual snowfall was derived from the bias-adjusted and
187 downscaled daily precipitation and air temperature fields and evaluated against annual snowfall from daily gridded
188 precipitation and air temperature datasets from MeteoSwiss (RhiresD and TabsD; MeteoSwiss (2016, 2017).
189 Snowfall fraction bias was calculated for each model chain as the difference between the simulated snowfall
190 fraction and the reference snowfall fraction.

191 Historical simulated SWE was evaluated against the SPASS-CL dataset (Marty et al., 2025; Michel et al., 2024).
192 For each model chain, the percentage bias in September-May mean and maximum SWE was computed at each
193 grid pixel relative to SPASS-CL. The resulting SWE simulations were further aggregated into 200 m elevation
194 bands between 800 and 2600 m a.s.l., corresponding to the elevation range over which SPASS-CL shows the best
195 agreement with observations (Marty et al., 2025). Biases in snowfall and SWE were assessed for all model chains,
196 both spatially and by binning in 200 m elevation bands. Model chains with mean SWE biases smaller than 10%
197 over the 800-2600 m a.s.l. elevation range were retained for future snow simulations, with two exceptions that are
198 discussed in the results.

199 After selecting the model chains that best reproduced SWE over the 1991-2020 reference period, the simulated
200 SWE fields of each model chain were statistically nudged through quantile mapping toward a reference SWE
201 dataset (SPASS-CLQM), which was produced with the same model but enhanced using data assimilation of snow
202 observations from 1998 onwards (Michel et al., 2024). The bias-adjusted SWE simulations were verified across
203 elevation bands to ensure that the correction produced a reliable snow climatology, before applying it to future
204 scenarios. The overall modeling workflow is described in Figure 2.



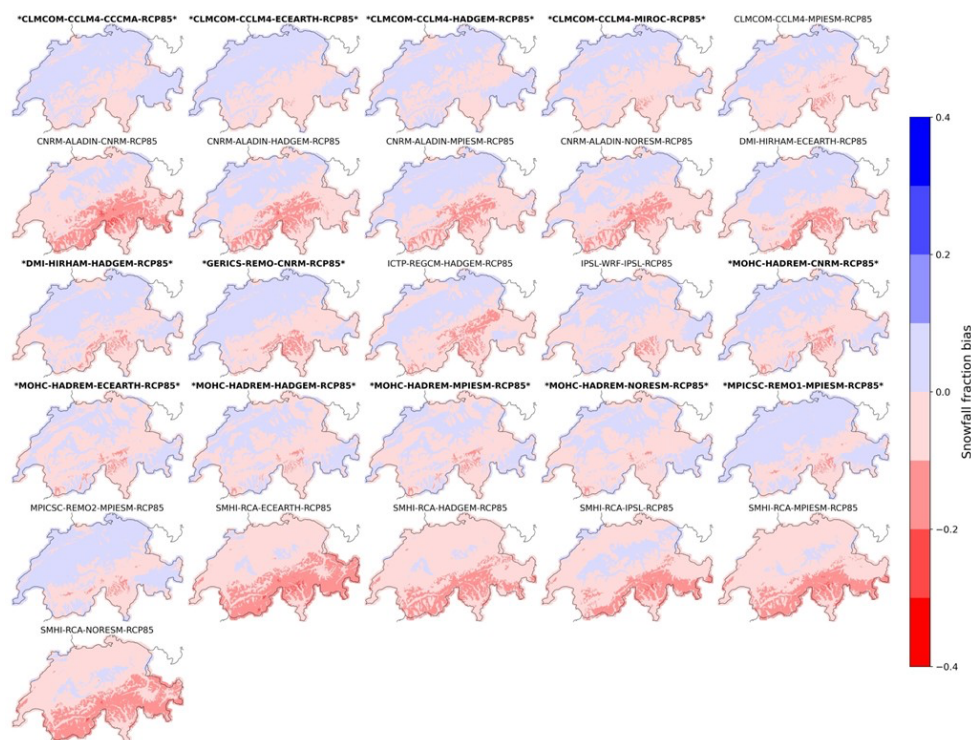
205
206 Figure 2: Flowchart describing the workflow to derive future snow projections.

207 **3 Results and Discussion**

208 **3.1 Biases in snowfall fraction and air temperature-precipitation relationships**

209 Biases in snowfall fraction showed a clear dependence on the regional climate model (RCM; Figure 3). As the
210 driving global climate model (GCM) provides the large-scale boundary conditions, the RCM process
211 parameterization, together with the subsequent statistical downscaling and bias adjustment, largely controlled the
212 spatial structure of snowfall fraction biases across Switzerland. This is consistent with previous evaluations of
213 EURO-CORDEX simulations over the European Alps, which showed that bivariate model biases in temperature
214 and precipitation at local scales are more influenced by RCMs (Matiu et al., 2024; Meyer et al., 2019). CLMCOM-
215 CCLM4 model chains generally showed the smallest snowfall fraction biases across different driving GCMs, with
216 the lowest overall bias found for the chain driven by CCCMA. In contrast, several CNRM-ALADIN and SMHI-
217 RCA model chains showed pronounced negative biases in the high-elevation Alpine region, with snowfall fraction
218 being underestimated by up to 40% (Figure 3).

219 Across the lower-elevation Swiss Plateau, most model chains showed relatively small snowfall fraction biases,
220 generally below 10%, consistent with previous evaluations of EURO-CORDEX snowfall fraction over the Alps
221 (Frei et al., 2018). The largest biases occurred in the high-elevation Alpine regions, where the bias-adjusted
222 Climate CH2025 ensemble tended to underestimate snowfall fraction during the 1991-2020 reference period. This
223 contrasts with earlier evaluations of raw EURO-CORDEX snowfall, which reported snowfall overestimation in
224 high-elevation Alps attributed partly to wet and cold RCM biases (Frei et al., 2018; Matiu et al., 2024). To
225 investigate this discrepancy, we compared the bivariate relationship between air temperature and precipitation in
226 the raw RCM output and in the bias-adjusted Climate CH2025 forcing fields.



227

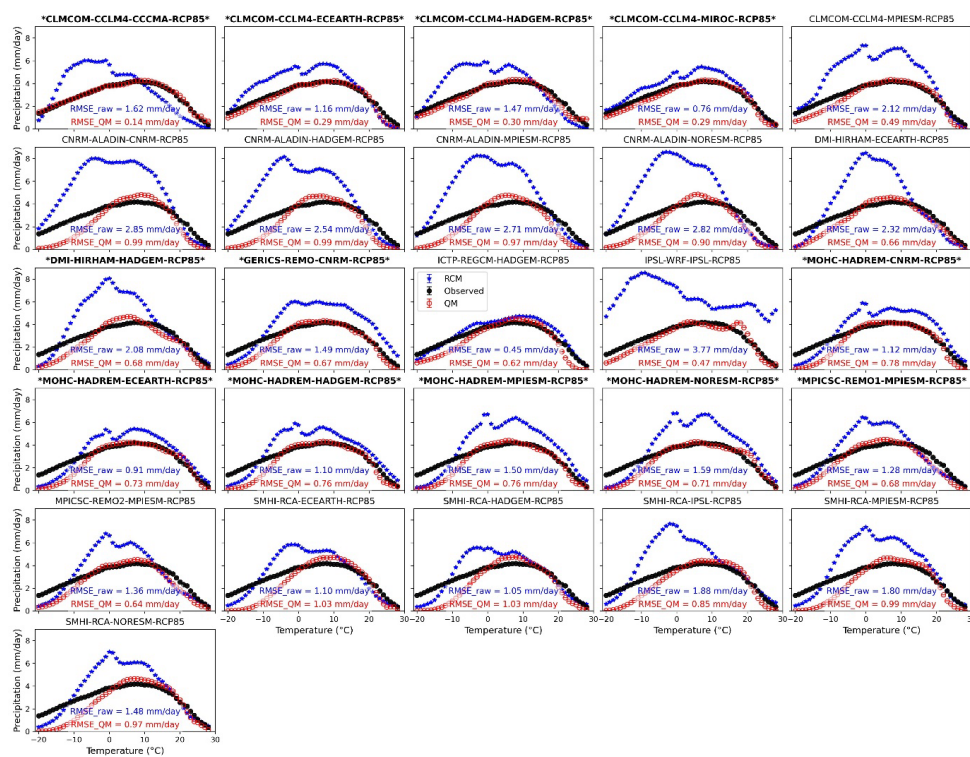
228 Figure 3: Bias in snowfall fraction for the 26 Climate CH2025 models relative to snowfall fraction estimated from
 229 observational gridded precipitation and temperature data (RhiresD and TabsD), for the reference period 1991-
 230 2020. Positive values indicate overestimation of snowfall fraction, while negative values indicate underestimation.
 231 Model chains retained for future SWE simulations are marked in bold with an asterisk mark (*). Model-chain
 232 labels follow the convention [RCM]-[GCM]-[RCP].

233 Temperatures below 0°C provide a first-order indication of conditions favorable for snowfall. The raw RCM
 234 outputs generally showed higher precipitation amounts at temperatures below 0°C than the observational reference
 235 (Figure 4), indicating a tendency toward simulating excessive precipitation under conditions favorable for
 236 snowfall. After univariate quantile mapping of precipitation and temperature, precipitation amounts in these colder
 237 temperature bins were systematically reduced across all model chains (Figure 4). The bias adjustment reduced the
 238 overall mismatch between simulated and observed precipitation-temperature relationships for most models, as
 239 indicated by lower root mean squared errors (RMSE). However, it also reduced precipitation specifically under
 240 sub-zero temperatures, thereby decreasing the simulated snowfall fraction.

241 These analyses help explain why the bias-adjusted CH2025 forcing fields produced negative snowfall fraction
 242 biases in Alpine regions, whereas earlier evaluations of raw EURO-CORDEX output reported positive snowfall
 243 fraction biases at higher elevations (Frei et al., 2018; Matiu et al., 2024). The result is also consistent with previous
 244 hydrological impact studies showing that univariate bias adjustment can alter snowfall and SWE estimates, as
 245 they do not preserve inter-variable relationships (Michel et al., 2021). For instance, Meyer et al., (2019) showed
 246 that univariate bias correction reduced snowfall and SWE compared with multivariate bias correction for partly



247 glacierized Swiss Alpine catchments, while Eum et al., (2020) reported similar effects in snow-dominated
 248 Athabasca River basin in Canada. Rätty et al., (2018) also reported that the clearest benefit of multivariate bias-
 249 adjustment vs univariate bias-adjustment was for variables which are jointly controlled by temperature and
 250 precipitation such as SWE and high streamflow.



251

252 Figure 4: Daily mean precipitation (mm/day) conditional on daily mean air temperature for the 26 Climate
 253 CH2025 model chains over 1991-2020. Precipitation was averaged with 1°C temperature bins from -20°C to 30°C
 254 across Switzerland. The raw RCM output was interpolated to 1x1 km² spatial resolution, whereas the Climate
 255 CH2025 forcing fields and observational references (RhiresD, TabsD) were already gridded at 1x1 km². Model
 256 chains retained for future SWE simulations are marked in bold with an asterisk mark (*). Model-chain labels
 257 follow the convention [RCM]-[GCM]-[RCP].

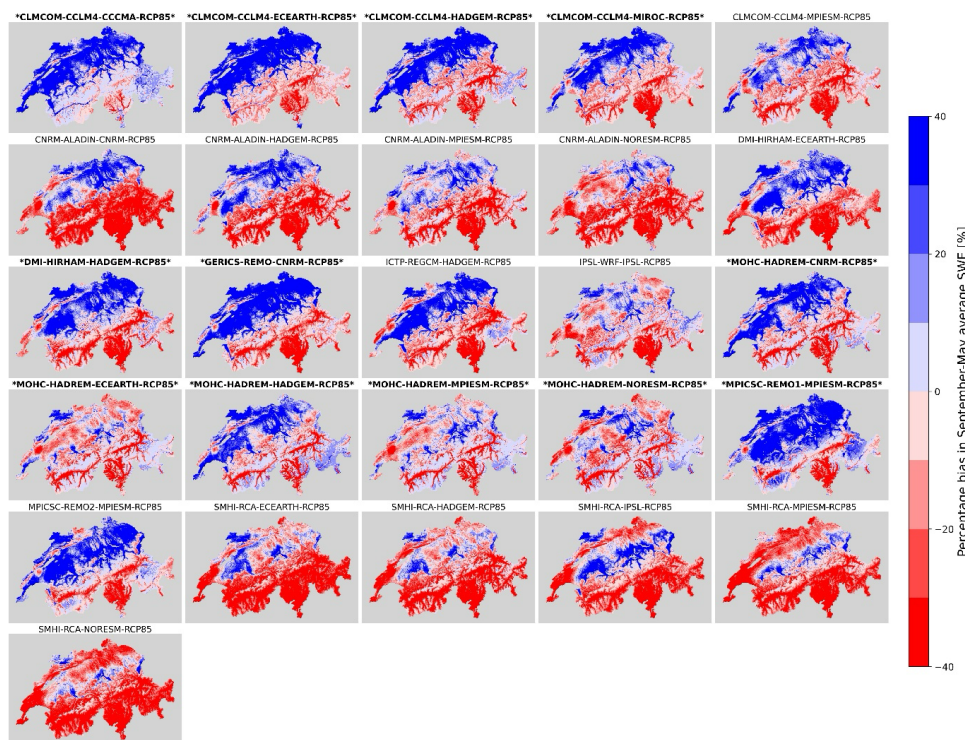
258 3.2 Biases in snow water equivalent (SWE) and propagation of biases from snowfall to SWE

259 We next evaluated how biases in annual snowfall fraction, representing only the atmospheric forcings, affected
 260 snow accumulation on the ground, quantified as September-May mean and maximum SWE. The spatial patterns
 261 of SWE biases in the reference period 1991-2020 (Figure 5) were broadly consistent, but larger, than the snowfall
 262 fraction biases shown in Figure 3, indicating that errors in snowfall accumulation propagated into simulated SWE.
 263 Spatial bias patterns were also similar among model chains sharing the same RCM but driven by different GCMs,
 264 further confirming that the RCM and the subsequent downscaling and bias-adjustment steps exerted a strong
 265 control on the historical SWE climatology. Several CLMCOM-CCLM4 model chains showed comparatively



266 small SWE biases, particularly in the higher-elevation Alpine regions, and most of the model chains retained for
 267 future SWE simulations were among those with the lowest reference-period SWE biases. In contrast, CNRM-
 268 ALADIN and SMHI-RCA model chains exhibited pronounced negative SWE biases across large parts of the
 269 Alpine domain, consistent with their negative snowfall fraction biases (Figure 3). Because mean SWE integrates
 270 snow accumulation and melt over the season, these negative SWE biases indicate that the underestimation of
 271 snowfall fraction translated directly into too little seasonal snow storage.

272 Several models showed positive SWE biases in lower-elevation regions of the Swiss Plateau (Figure 5). These
 273 biases should be interpreted with caution as snow occurrence in these regions is intermittent and mean SWE values
 274 are very small (Marty et al., 2025; Michel et al., 2024). Therefore, percentage biases can become large even when
 275 absolute differences are minor. In addition, the SPASS-CL reference dataset is not reliable at lower elevations
 276 (Marty et al., 2025). For this reason, model selection for future runs was based primarily on performance across
 277 the 800-2600 m a.s.l. elevation range, where SPASS-CL provides the most reliable benchmark for simulated
 278 SWE.



279

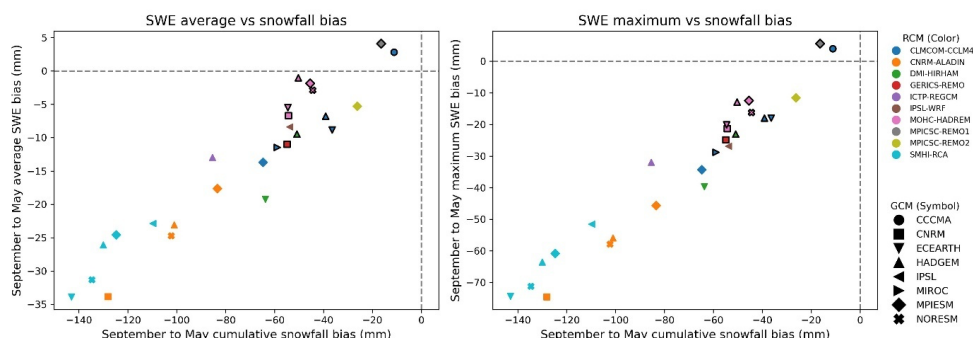
280 Figure 5: Percentage bias in September-May mean snow water equivalent (SWE) for the 26 Climate CH2025
 281 models relative to the SPASS-CL reference dataset over 1991-2020. Positive values indicate SWE overestimation
 282 and negative values indicate SWE underestimation. Model chains retained for future SWE simulations are marked
 283 in bold with an asterisk mark (*). Model-chain labels follow the convention [RCM]-[GCM]-[RCP].



284 Averaged over September–May and across the 800–2600 m a.s.l. elevation range, all Climate CH2025 model
285 chains showed negative snowfall fraction biases relative to the observational gridded precipitation and
286 temperature data (Figure 6). These snowfall biases propagated almost linearly into both mean and maximum SWE
287 biases, suggesting that bias in snowfall accumulation was the primary control on SWE bias (Figure 6). Consistent
288 with the systematic underestimation of snowfall fraction, 24 out of the 26 model chains also underestimated both
289 mean and maximum SWE during the 1991–2020 reference period. This strong link between snowfall and SWE
290 biases underlines the importance of evaluating climate models with process-relevant indicators, rather than only
291 with the marginal distributions of temperature and precipitation. Such process-oriented model evaluation has also
292 been advocated for hydrological applications, where climate model biases can be amplified or compensated
293 through nonlinear snow and runoff processes (Hakala et al., 2018).

294 Model selection was based on their joint performance for simulating snowfall fraction, mean SWE, and maximum
295 SWE, averaged across Switzerland over September–May period during 1991–2020. In terms of exact criterion,
296 model chains with mean SWE biases within $\pm 10\%$ were retained for future simulations (Figures 6, S1), with two
297 exceptions described in the next paragraph. All MOHC-HADREM models showed comparatively smaller biases
298 in snowfall fraction, mean SWE, and maximum SWE, and were retained. Four out of the five CLMCOM-CCLM4
299 models were also retained for future runs because of their relatively lower errors across snowfall fraction, mean
300 SWE, and maximum SWE. The largest negative snowfall and SWE biases occurred for the CNRM-ALADIN and
301 SMHI-RCA model chains (Figure 6). These RCMs, after bias adjustment, produced too little seasonal snow
302 accumulation over the reference period and were excluded from the future SWE simulations.

303 Two exceptions were made in the model selection criterion. First, only one of the two MPICSC-REMO
304 realizations was retained (Figure 6). Both realizations were driven by the same GCM boundary forcing (MPIESM)
305 and used the same RCM formulation (MPICSC-REMO), resulting in similar snowfall and SWE behavior. To
306 avoid giving disproportionate weight to this model, we retained only the realization with the smallest snowfall
307 and SWE biases. Second, the IPSL-WRF model chain driven by IPSL boundary conditions was excluded despite
308 its reasonable reference-period snow simulation. Based on percentage biases, IPSL-WRF was only slightly less
309 accurate to the next-best selected model chain, and its SWE bias in millimeters was well within the ensemble
310 spread. However, this model chain showed an outlying future climate-change signal for 2070–2099 relative to the
311 reference period (1991–2020), including a 60% projected increase in summer precipitation and the smallest
312 projected summer warming of only 2°C (Figure 8). Because this response is not representative of the broader
313 Climate CH2025 ensemble and was identified as an outlier model in the CH2025 scientific report, the model chain
314 was excluded from future SWE simulations. This type of performance-based sub-selection is consistent with
315 previous recommendations that climate model ensembles used for impact studies should be evaluated for the
316 specific processes and variables relevant to the target application (Hakala et al., 2018; Peßenteiner et al., 2021).



317

318 Figure 6: Relationship between snowfall fraction and SWE bias for the 26 Climate CH2025 model chains over
 319 the 1991-2020 reference period. Biases were averaged over September-May and over the 800-2600 m a.s.l.
 320 elevation range. The left and right panels show the relationship between snowfall fraction bias and biases in mean
 321 and maximum SWE, respectively. Point color indicates the RCM, while point shape indicates the driving GCM.
 322 Points with a black outline denote model chains retained for future SWE runs.

323 3.3 Quality of the selected ensemble of models for future snow scenarios

324 The models selected for future snow simulations generally showed September-May mean SWE biases within
 325 $\pm 10\%$ across most elevation bands between 800-2600 m a.s.l. (Figure 7). Percentage biases at low elevations
 326 should be interpreted with caution because snow accumulation is small and intermittent in these regions.
 327 Consequently, small absolute SWE differences can translate into large percentage biases, with limited impact on
 328 seasonal meltwater availability relative to the annual water balance.

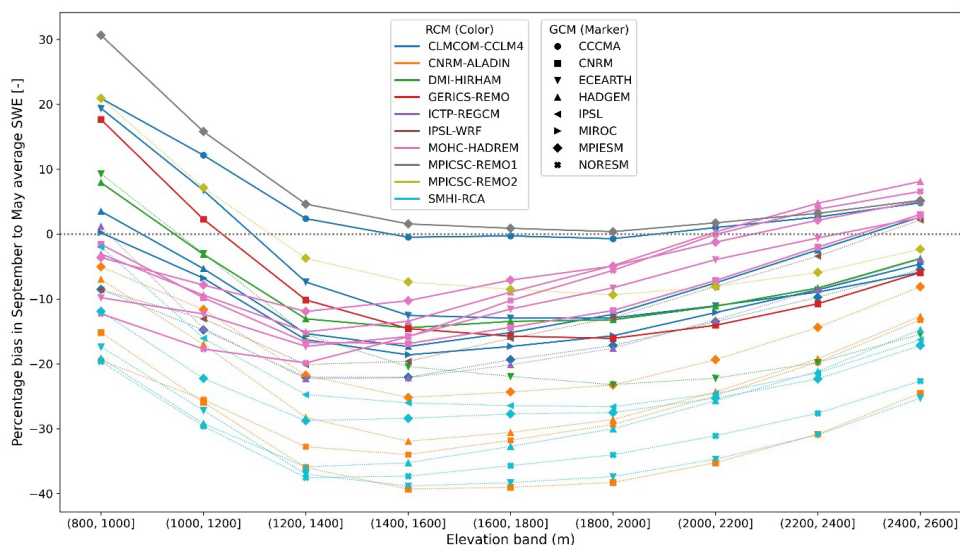
329 Among the selected models, CLMCOM-CCLM4-CCCMA showed the lowest overall bias across most elevation
 330 bands, suggesting that it best captured the observed elevation-dependent snow accumulation pattern over
 331 Switzerland (Figure 7). This is consistent with a very close match in precipitation-temperature bivariate
 332 relationship to the observational reference (Figure 4). MOHC-HADREM model chains showed significant
 333 negative percentage biases below 1400 m a.s.l., often exceeding $\pm 10\%$ threshold, but their performance improved
 334 above 1600 m a.s.l., resulting in acceptable SWE simulations over the full elevation range. MPICSC-REMO2 was
 335 the only model chain with biases largely within $\pm 10\%$ that was nevertheless excluded, because the closely related
 336 MPICSC-REMO1 realization was already retained and showed slightly smaller snowfall and SWE biases. In
 337 contrast, CNRM-ALADIN and SMHI-RCA model chains showed the largest negative biases across most
 338 elevation bands (Figure 7), consistent with insufficient snowfall accumulation across the Swiss domain (Figures
 339 3, 6).

340 The elevation-band analysis also illustrates that GCM boundary conditions can sometimes influence SWE
 341 simulations even when the same RCM is used and even given the fact that all simulations were bias-adjusted
 342 towards observations for the 1991-2020 period. For example, DMI-HIRHAM driven by HADGEM
 343 conditions produced more realistic SWE during the reference period than DMI-HIRHAM driven by ECEARTH.
 344 Similarly, the CLMCOM-CCLM4 model driven by MPIESM boundary conditions showed larger percentage
 345 SWE biases than the other CLMCOM-CCLM4 model chains driven by three different GCMs, which generally



346 produced acceptable SWE simulations. This confirms that both the RCM formulation and the large-scale forcing
 347 can affect snow variables, even after statistical downscaling and bias adjustment. Similar dependence on the
 348 GCM-RCM pairing has been reported for Alpine climate biases and hydrological performance evaluations
 349 (Hakala et al., 2018; Matiu et al., 2024).

350 A notable feature of the elevation profiles is that negative percentage mean SWE biases were often largest between
 351 approximately 1400 and 1800 m a.s.l. This elevation range lies close to the transition between rain-dominated and
 352 snow-dominated regimes, where small biases in temperature, precipitation, or precipitation phase can strongly
 353 affect snow accumulation. This is also the elevation range where previous studies have shown snow conditions to
 354 be particularly sensitive to warming and where transitions from seasonal to intermittent snow regimes are expected
 355 (Schmucki et al., 2015; Verfaillie et al., 2018). The concentration of high biases in this zone suggests that these
 356 elevations may be especially sensitive to limitations in precipitation phase partitioning and bias-adjusted forcing
 357 fields. A targeted evaluation of snow accumulation processes in these transitional elevation bands would therefore
 358 be valuable in future work.



359

360 Figure 7: Elevational dependence of September-May mean SWE percentage bias for the 26 Climate CH2025
 361 models over the 1991-2020 reference period. Biases are expressed relative to SPASS-CL and aggregated into 200
 362 m elevation bands from 800-2600 m a.s.l. Solid lines indicate model chains retained for future SWE simulations,
 363 while dotted thin lines indicate model chains excluded from future simulations. A similar plot for maximum SWE
 364 percentage bias is shown in Figure S2.

365 3.4 Future climate-change signals of the selected model ensemble

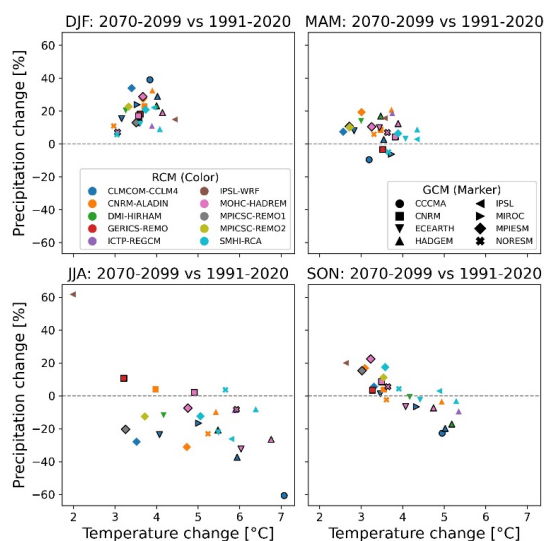
366 After selecting 12 model chains for future SWE simulations based on their 1991-2020 snow simulations, we
 367 evaluated whether this subset retained a representative range of future precipitation and temperature change
 368 signals from the full Climate CH2025 ensemble (Figure 8). This step is important because selecting models based



369 on historical snowfall and SWE biases could unintentionally narrow the range of projected future climate
 370 conditions and therefore change the range of simulated future snow changes.

371 The selected subset captured most of the ensemble spread in winter and spring precipitation and temperature
 372 change, which are the most relevant seasons for snow accumulation and melt. One exception is spring temperature,
 373 where the warmest model chains were not retained, implying that the snow ensemble was limited to spring
 374 warming levels of up to 4°C by end of century, and did not capture the warmest 4.5°C spring warming scenario.
 375 All models projected increases in winter precipitation, and most projected increases in spring precipitation.
 376 Combined with 2.5 to 4.5°C higher winter and spring temperatures, future cold-season precipitation will likely
 377 occur under warmer conditions, increasing the likelihood of a larger fraction of precipitation falling as rainfall
 378 rather than snowfall (MeteoSwiss and Zurich, 2025). This may also increase liquid-water inputs to the snowpack,
 379 with more instances of rain-on-snow flooding and wet-snow avalanches, which should be investigated in the future
 380 (Mayer et al., 2024).

381 The selected subset excludes the model chain with the highest projected increase in summer precipitation (IPSL-
 382 WRF-IPSL) but has limited relevance for SWE accumulation or melt, which primarily occurs during winter and
 383 spring conditions. In autumn, the ensemble shows a linear relationship between temperature and precipitation
 384 changes, with warmer model chains projecting lower future precipitation. Such a relationship is less evident in
 385 winter and spring, where most model chains project wetter conditions despite substantial warming. This is broadly
 386 consistent with earlier analyses which found that summer warming is often associated with stronger drying,
 387 whereas winter changes are more strongly characterized by increasing precipitation (Kotlarski et al., 2023).
 388 Overall, the selected model subset retains the main snow-season climate-change signals of the full ensemble while
 389 excluding model chains with poor reference-period snow simulations.



390

391 Figure 8: Projected seasonal changes in precipitation and air temperature for the 26 Climate CH2025 RCP8.5
 392 model chains for 2070-2099 relative to 1991-2020. Changes are shown for winter (DJF), spring (MAM), summer

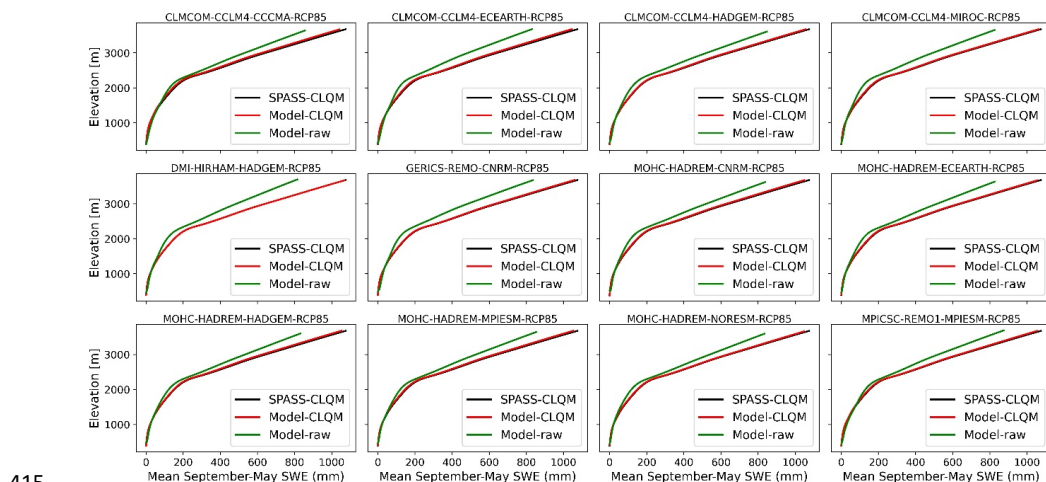


393 (JJA), and autumn (SON). Point color indicates the RCM, while point shape indicates the GCM. Model chains
 394 retained for future SWE simulations have black outlines.

395 **3.5 Quantile mapping of snow water equivalent (SWE) towards SPASS-CLQM**

396 Although the retained model chains showed better reference-period snow simulations than the full Climate
 397 CH2025 ensemble, substantial SWE biases remained, particularly in the high-elevation Alpine regions (Figures
 398 5, 9). For example, all 12 selected model chains underestimated September-May mean SWE above 1500 m a.s.l.,
 399 with negative biases becoming more pronounced above 2000 m a.s.l. (Figure 9). This pattern is consistent with
 400 negative snowfall fraction biases and indicates that insufficient snow accumulation in the meteorological forcing
 401 propagated into the lower SWE (Figure 6). Biases above 3000 m a.s.l. should be interpreted with caution because
 402 observational reference datasets are very uncertain at these elevations (Marty et al., 2025; Michel et al., 2024).

403 To reduce these residual biases, correction factors were derived for each quantile of the simulated SWE of each
 404 model chain in the reference period based on SPASS-CLQM, the best available gridded SWE reference for
 405 Switzerland. SPASS-CLQM is based on the same snow model but is enhanced through data assimilation of
 406 additional snow observations. After correcting the individual quantiles, SWE biases were substantially reduced
 407 across the selected model chains and became more closely aligned with SPASS-CLQM across elevations (Figure
 408 9). This is consistent with the previous studies showing that quantile mapping can strongly reduce seasonal mean
 409 SWE biases in Switzerland, although residual errors can remain at shorter timescales and in specific regions
 410 (Michel et al., 2024). We therefore applied the same SWE bias adjustment step to the future simulations to limit
 411 the influence of reference-period snow accumulation biases arising from the combined effects of raw RCM biases
 412 and univariate quantile mapping on precipitation and temperature forcings. This ensures that projected SWE
 413 changes are estimated from a snow climatology that is consistent with the best available observation-constrained
 414 reference dataset.



415
 416 Figure 9: Elevation dependence of September-May mean SWE bias before and after quantile mapping of
 417 simulated SWE for the 12 model chains retained for future scenarios. Biases are expressed as percentage

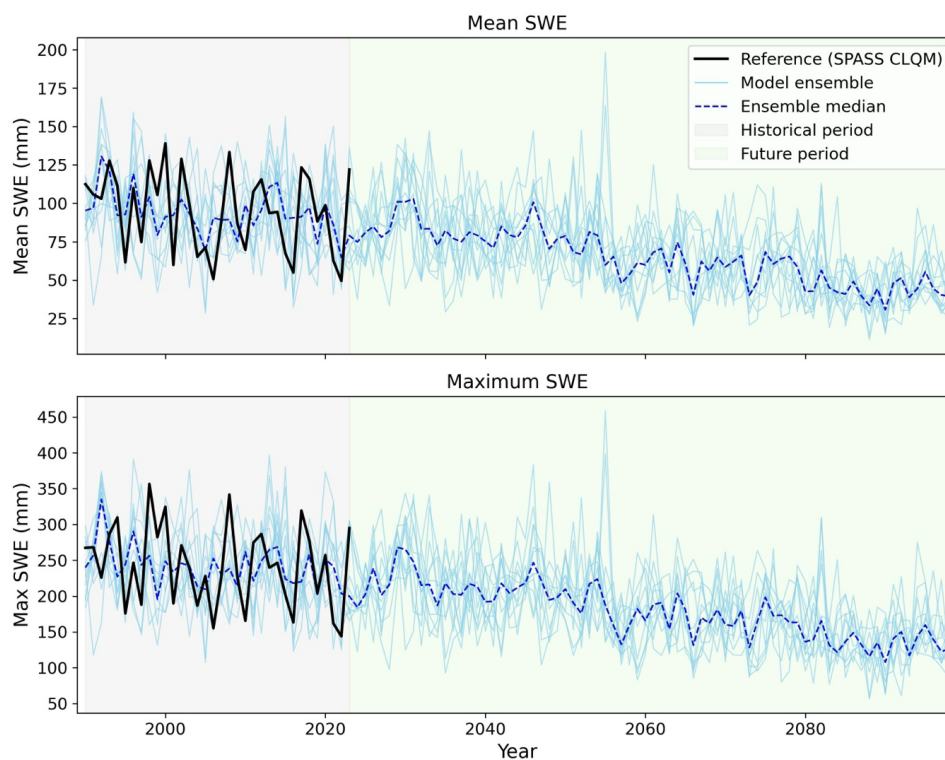


418 differences relative to the SPASS-CLQM reference dataset over the 1991-2020 reference period. A similar plot
419 for maximum SWE percentage bias is shown in Figure S3.

420 **3.6 Future projected changes in mean and maximum snow water equivalent (SWE)**

421 During the 1991-2020 reference period, the selected model ensemble reproduced the observed range of
422 interannual variability in both September-May mean and maximum SWE, as confirmed by the reference SPASS-
423 CLQM dataset (Figure 10). The selected model chains therefore provide a realistic representation of historical
424 year-to-year SWE variability after bias adjustment. The ensemble median shows lower variability than both the
425 reference dataset and the individual model chains, which is expected because interannual fluctuations are not
426 synchronized among different climate models, resulting in lower variability of the ensemble median. For this
427 reason, the full ensemble envelope is more informative than the median alone when assessing plausible future
428 conditions and year-to-year variability.

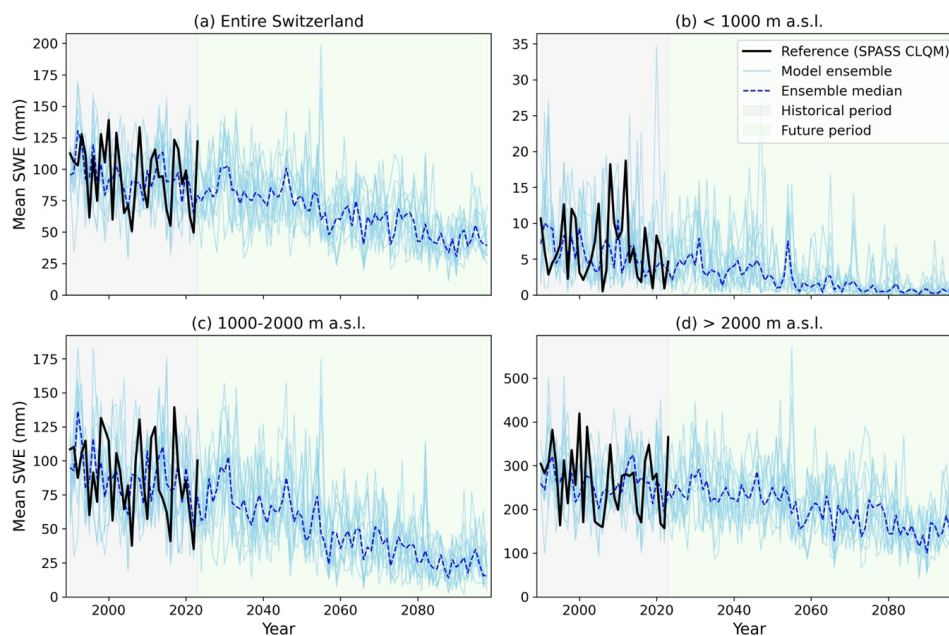
429 Both mean and maximum SWE are projected to decline throughout the 21st century. However, the decline in the
430 long-term mean SWE does not imply a disappearance of interannual variability. Large year-to-year fluctuations
431 persist through the future period, and some individual years show maximum SWE values comparable to, or even
432 exceeding, the highest SWE seen during 1991-2020 (Figure 10). This indicates that snow-rich winters can still
433 occur in a warmer climate, even as average snow storage decreases substantially. The projected signal should
434 therefore be interpreted as a shift toward lower typical SWE conditions, rather than a uniform reduction in SWE
435 every year. Until mid-century, SWE reductions are relatively moderate compared with end of century, when SWE
436 losses intensify. This is consistent with snow projections in previous Alpine studies, where interannual variability
437 remained substantial even as median snow conditions declined, with higher SWE decline toward the end of the
438 century in the highest emission scenario (Kotlarski et al., 2023; Verfaillie et al., 2018).



439

440 Figure 10: Temporal evolution of September-May mean SWE (top) and maximum SWE (bottom) averaged across
441 Switzerland for the 12 selected Climate CH2025 model chains and for the RCP8.5 greenhouse gas scenario. The
442 1991-2024 period is shaded in gray, and the future projection period is shaded in light green. The black line shows
443 the SPASS-CLQM reference dataset for the historical period. Individual model simulations are shown in cyan,
444 and the ensemble median is shown as a dashed violet line.

445 Projected SWE losses show a strong elevation dependence (Figures 11-13). The lower elevation parts of
446 Switzerland below 1000 m a.s.l. are projected to become nearly snow-free by the end of the 21st century under
447 high RCP8.5 emissions (Figures 11b, 12). In these regions, substantial SWE losses are already apparent by mid-
448 century, with mean SWE reduced by more than 50% and maximum SWE declining by 30-50% (Figure 13). By
449 2069-2099, mean September-May SWE is projected to decrease by more than 80%, with corresponding maximum
450 SWE reductions of 60-80%. These results are consistent with previous Swiss and Alpine snow projections.
451 Schmucki et al., (2015) and Marty et al., (2017a) projected end-century snow reductions of about 95% at about
452 500 m a.s.l., while Kotlarski et al., (2023) projected SWE losses exceeding 80% across large parts of Alpine
453 forelands under RCP8.5. These changes indicate a transition toward increasingly rare and short-lived snow
454 conditions in the lower-elevation Swiss Plateau.



455

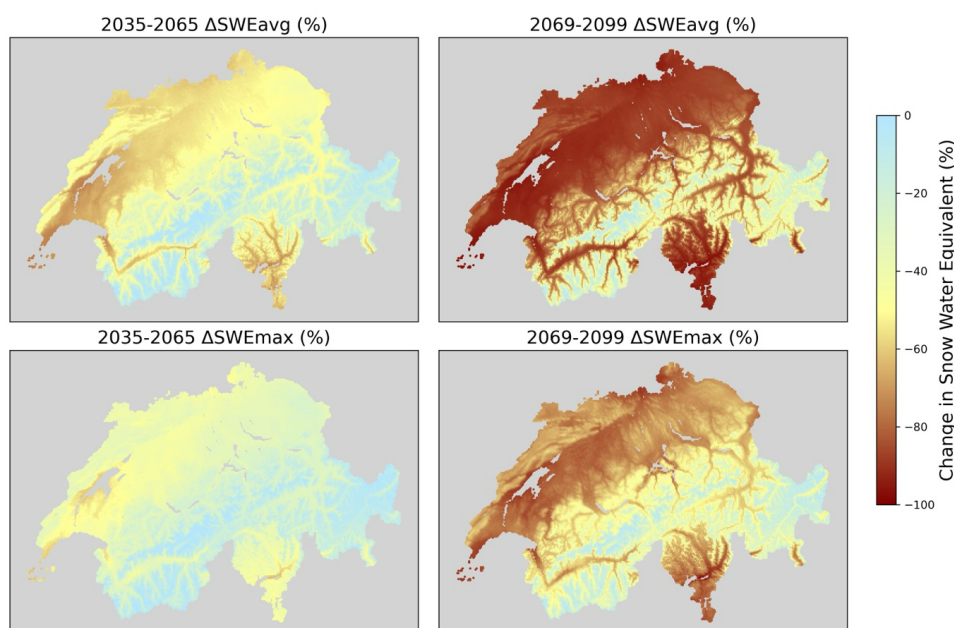
456 Figure 11: Temporal evolution of September-May mean SWE from 1991 to 2099 for the 12 selected Climate
 457 CH2025 model chains, all of them assuming the RCP8.5 greenhouse gas scenario. SWE is averaged over (a)
 458 Switzerland, (b) elevations below 1000 m a.s.l., (c) elevations between 1000 and 2000 m a.s.l., and (d) elevations
 459 above 2000 m a.s.l. The 1991-2024 period is shaded in gray, and the future projection period is shaded in light
 460 green. The black line shows the SPASS-CLQM reference dataset for the historical period. Individual model
 461 simulations are shown in cyan, and the ensemble median is shown as a dashed violet line. The corresponding
 462 temporal evolution of September-May maximum SWE is shown in Figure S4.

463 Intermediate elevations between 1000 and 2000 m a.s.l. also show strong SWE reductions, but with larger spatial
 464 and ensemble variability (Figures 11-13). By 2069-2099, mean SWE decreases by 50-90%, while maximum SWE
 465 decreases by 30-80%. This wide range suggests that different parts of this elevation zone will undergo different
 466 transitions: some areas are likely to shift toward intermittent or ephemeral snow regimes, whereas others may still
 467 maintain a seasonal snowpack, albeit with substantially reduced accumulation and persistence. This is in-line with
 468 previous station-based snow simulations for Switzerland, which projected that mid-elevation snowpacks between
 469 1000-1700 m a.s.l. will become increasingly ephemeral by end of the century (Schmucki et al., 2015). It is also
 470 consistent with snow projections in the Chartreuse mountain range in the Northern French Alps at 1500 m a.s.l.,
 471 where high-emission scenarios lead to increasingly frequent ephemeral or nearly snow-free conditions in the late
 472 21st century (Verfaillie et al., 2018).

473 Even higher elevation regions above 2000 m a.s.l. are projected to experience substantial SWE losses, with mean
 474 SWE decrease of 20-70%, and maximum SWE decreases of 15-60%, depending on the specific elevation band.
 475 The smallest relative reductions occur at the highest elevations, where colder winter conditions allow a larger
 476 fraction of precipitation to remain as snow. Increasing winter precipitation may partly buffer SWE losses in these

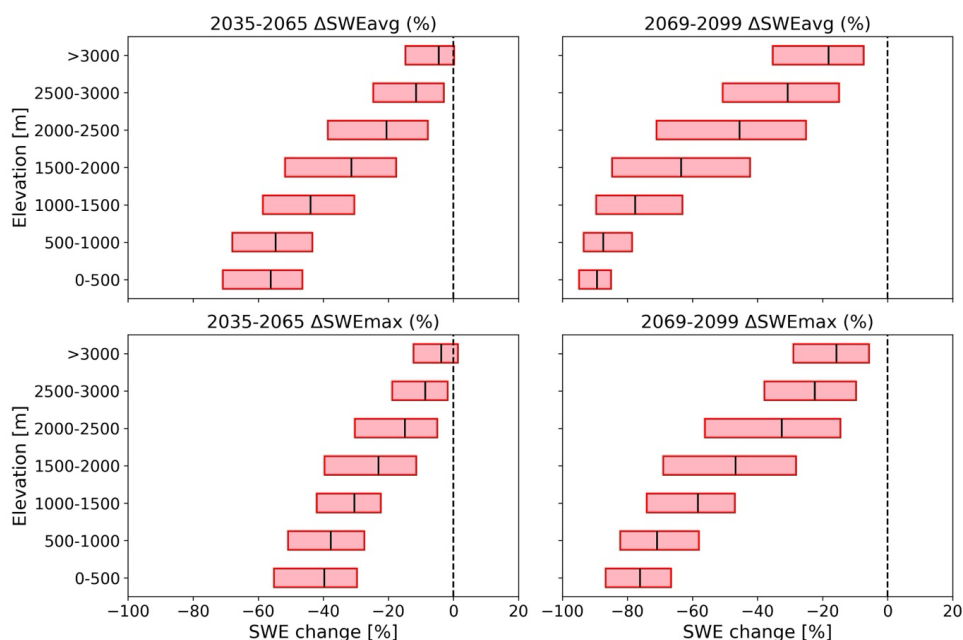


477 high-elevation regions, as suggested by the weaker reductions in the upper elevation bands in Figure 13 (Frei et
478 al., 2018). This is consistent with previous Alpine snow projections, which showed that relative SWE losses
479 became smaller with increasing elevation in high emission scenarios (Kotlarski et al., 2023). However, projections
480 at very high elevations should be interpreted with caution because snow observations are sparse, glacierized areas
481 form an important component of the water balance, and glacier processes are not represented in the present
482 modeling setup. Furthermore, the raw RCM simulations do not cover elevations above about 3000 m. A follow-
483 up study with explicit glacier representation and improved high-elevation forcing constraints would be needed to
484 assess these regions more robustly.



485

486 Figure 12: Projected percentage change in September-May mean (top row) and maximum (bottom row) SWE
487 across Switzerland relative to the 1991-2020 reference period and for the RCP8.5 greenhouse gas scenario.
488 Changes are shown for the near future (2035-2065; left column) and the end of the century (2069-2099; right
489 column), based on the ensemble median of the 12 selected Climate CH2025 models. Grid cells with September-
490 May mean across the ensemble below 1mm during 1991-2020 are shown in gray.



491

492 Figure 13: Elevation dependence of projected percentage change in September-May mean SWE (top row) and
 493 maximum SWE (bottom row) relative to 1991-2020 reference period and for the RCP8.5 greenhouse gas scenario.
 494 Changes are aggregated into elevation bands and shown for the near future (2035-2065; left column) and the end
 495 of the century (2069-2099; right column). Boxes refer to the 5th-95th percentile range across the 12 selected
 496 Climate CH2025 model chains, and vertical lines indicate the ensemble median.

497 **4 Limitations and future opportunities**

498 **4.1 Degree-day based snow modeling**

499 The projected SWE changes should be interpreted considering the uncertainty associated with the snow model
 500 structure. The spatially distributed temperature-index model on a 1km grid used in this study is computationally
 501 efficient and therefore well suited for national-scale ensemble projections. However, it does not explicitly resolve
 502 the full surface energy balance, lacks a detailed representation of forest canopy processes, does not account for
 503 slope- and aspect-dependent surface energy inputs, and neglects wind-driven snow redistribution and glacier mass
 504 balance. Because the simulations were driven only by gridded precipitation and air temperature, the model cannot
 505 resolve local differences in snow accumulation and melt, for example, between north- and south-facing slopes
 506 within the same elevation band. These limitations are important because model structural uncertainty can be
 507 substantial in complex mountain terrain. Recent work has shown that differences in snowmelt method, land-cover
 508 representation, and spatial resolution can be comparable in magnitude to the effect of a 1°C warming in complex
 509 mountain terrain (Rottler et al., 2026). Temperature-index snow models may also underestimate melt during rain-
 510 on-snow events, when turbulent fluxes can become more important (Mott et al., 2023). Our simulations may



511 therefore underestimate the role of snowmelt during future rain-on-snow events, particularly in elevation bands
512 where warmer winters increase the frequency of liquid precipitation on snow.

513 To reduce systematic biases in simulated snow storage, we bias-adjusted SWE toward SPASS-CLQM, the best
514 available observation-constrained climatological SWE dataset for Switzerland, which substantially reduced
515 reference-period SWE biases across elevation bands. Nevertheless, the correction cannot fully compensate for
516 missing physical processes resulting in additional uncertainties in snow accumulation and ablation dynamics. The
517 projected SWE losses and its elevation dependence are robust and consistent with previous Alpine studies, but the
518 exact magnitude of change can have biases in topographically complex terrains, forested regions, glacierized
519 catchments, and during rain-on-snow events. Future work should assess these sensitivities using energy-balance
520 snow models driven by higher-resolution meteorological forcing.

521 **4.2 Univariate quantile mapping of meteorological forcings**

522 An important limitation arises from the univariate quantile mapping for producing daily precipitation and
523 temperature fields at 1×1 km² resolution in the Climate CH2025 project. This bias-adjustment step substantially
524 improves the marginal distributions of these variables compared with raw EURO-CORDEX outputs. However,
525 univariate correction treats precipitation and temperature independently and therefore does not explicitly preserve
526 their joint dependence, which is particularly important for snow applications, because snowfall is controlled by
527 the co-occurrence of precipitation at near-freezing or sub-freezing temperatures.

528 Our analysis revealed that the raw EURO-CORDEX outputs generally produced too much precipitation at
529 temperatures below 0°C relative to observations, whereas the univariate bias-adjusted Climate CH2025 forcings
530 systematically reduced precipitation in these cold-temperature bins. Although this correction improved the overall
531 precipitation-temperature bivariate relationship, it reduced snowfall fraction in Alpine regions and led to negative
532 snowfall biases, which then propagated almost linearly into negative mean and maximum SWE biases. This
533 behavior is consistent with previous studies showing that univariate bias-adjustment can distort snowfall and SWE
534 in snow-dominated landscapes, whereas multivariate approaches can better preserve precipitation-temperature
535 dependencies (Astagneau et al., 2025; Eum et al., 2020; Meyer et al., 2019).

536 We addressed this limitation in two ways: first, by selecting the Climate CH2025 model chains that best
537 reproduced snowfall fraction and SWE during the 1991-2020 reference period, and second, by quantile mapping
538 simulated SWE toward the SPASS-CLQM reference dataset. These steps reduced reference-period SWE biases
539 across elevations and improved the snow climatology used for future projections. Nevertheless, they cannot fully
540 recover physically consistent precipitation-temperature dependence in the underlying meteorological forcing.
541 Future generations of national climate scenarios intended for snow applications should therefore consider
542 multivariate bias-adjustment techniques that explicitly preserve precipitation-temperature dependence.
543 Incorporating additional snow observations, such as snow depth or new snow height, directly into the bias-
544 adjustment workflow could further improve the consistency of climate forcings for snow impact studies.



545 **4.3 Mapping transient snow scenarios to global warming levels**

546 The Climate CH2025 scenarios express future climate changes primarily in terms of Global Warming Levels
547 (GWLs), by mapping transient climate-model simulations to periods corresponding to specified levels of global
548 mean warming (MeteoSwiss and Zurich, 2025). In this study, we instead analyzed transient SWE projections from
549 a selected subset of 12 RCP8.5 model chains, which were retained because they reproduced reference-period
550 snowfall and SWE more realistically than the full CH2025 ensemble. However, because of the smaller ensemble
551 size relative to the Climate CH2025 scenarios, the GWL framework cannot be transferred directly to the adjusted
552 subset. As the snow ensemble only included the highest emission scenarios (RCP8.5), it ensures that each model
553 within the ensemble will reach higher warming levels, including 3°C, until 2100, which may not be reached under
554 lower-emission pathways. A natural next step is therefore to map the bias-adjusted transient SWE simulations
555 onto the same GWL framework used in Climate CH2025. Such a GWL-based framing would make the SWE
556 projections directly comparable with other Climate CH2025 impact indicators and more useful for adaptation
557 planning. It will be the subject of a follow-up study.

558 **5 Conclusions**

559 This study provides daily 1×1 km² projections of snow water equivalent (SWE) for Switzerland using bias-
560 adjusted Climate CH2025 meteorological forcings, a spatially distributed temperature-index snow model, and an
561 observation-constrained long-term SWE reference dataset. We showed that the univariate quantile mapping of
562 Climate CH2025 precipitation and temperature improved the marginal distributions of these variables, but
563 systematically reduced precipitation under sub-freezing conditions. This led to negative snowfall fraction biases
564 in Alpine regions, which propagated into negative biases in both mean and maximum SWE. To reduce these
565 effects, we retained 12 model chains from the 26 available Climate CH2025 models based on their ability to
566 reproduce snowfall fraction, mean SWE, and maximum SWE during the 1991-2020 reference period. For these
567 selected models, simulated SWE was further quantile mapped toward SPASS-CLQM, the best available
568 observation-constrained long-term SWE dataset for Switzerland, resulting in a more realistic elevation-dependent
569 SWE climatology that was then used for future simulations.

570 The future simulations – all of them assuming the high RCP8.5 greenhouse gas scenario – indicate widespread
571 SWE decreases across Switzerland, while year-to-year variability remains large and comparable to the reference
572 period. Individual snow-rich winters can still occur in the future, occasionally reaching SWE values comparable
573 to high-SWE years during 1991-2020. However, both mean and maximum SWE would decline throughout the
574 21st century. The projected change should therefore be interpreted as a shift toward lower typical snow storage,
575 rather than a uniform reduction of SWE every year.

576 Projected SWE losses are strongly elevation dependent, with the largest percentage of SWE reductions at low
577 elevations. By the end of 21st century, mean SWE losses are projected to exceed 80% below 1000 m a.s.l.,
578 indicating a transition toward increasingly rare and short-lived snow conditions in low-elevation Switzerland. At
579 intermediate elevations between 1000 and 2000 m a.s.l., mean SWE are projected to reduce by 50-90%, with
580 many regions likely shifting toward more ephemeral snowpacks. Even above 2000 m a.s.l., mean SWE is expected
581 to decrease by 20-70%, suggesting that even high-elevation seasonal snow storage will get substantially reduced.



582 These projections provide a spatially detailed basis for assessing future changes in Swiss snow resources and for
583 supporting adaptation in hydrology, ecology, natural hazards, and snow-dependent economic sectors. However,
584 uncertainties remain from the use of a temperature-index snow model, the lack of explicit glacier and energy-
585 balance processes, and limitations of univariate meteorological bias adjustment. Future work should therefore
586 explore multivariate or snow-constrained bias adjustment techniques, energy-balance snow modeling, explicit
587 glacier coupling, and the mapping of transient SWE projections to the Global Warming Level framework used in
588 Climate CH2025.

589 **Data availability**

590 Daily gridded precipitation and temperature timeseries from Climate CH2025 model chains are freely available
591 as a part of the Open Government Data at <https://opendatadocs.meteoswiss.ch/c-climate-data>. Modelled
592 historical SWE data (SPASS-CLQM) are available at <https://doi.org/10.16904/envidat.580>. The modelled future
593 SWE timeseries are available on envidat.ch (URL to be provided upon publication).

594 **Author contribution**

595 HB: conceptualization, data curation, formal analysis, methodology, software, visualization, writing – original
596 draft preparation, writing – review and editing; SK: conceptualization, methodology, supervision, funding
597 acquisition, writing – review and editing; AM: methodology, software, resources, writing – review and editing;
598 JM: writing – review and editing; CM: conceptualization, methodology, supervision, funding acquisition, writing
599 – review and editing.

600 **Competing interests**

601 The authors declare that they have no conflict of interest.

602 **Acknowledgements**

603 We thank Tobias Jonas (SLF) for his substantial support with snow modeling, guidance in interpreting the results,
604 and valuable advice throughout the project. We thank Michael Herrmann (MeteoSwiss) for his support in
605 compiling and bias correcting Climate CH2025 models.

606 **Financial support**

607 This research was supported by MeteoSwiss (in the frame of the Climate CH2025 project) and WSL (grant number
608 #202401N2769).

609



610 **References**

- 611 Astagneau, P. C., Wood, R. R., Vrac, M., Kotlarski, S., Vaittinada Ayar, P., François, B., and Brunner, M. I.:
612 Impact of bias adjustment strategy on ensemble projections of hydrological extremes, *Hydrol. Earth Syst. Sci.*,
613 29, 5695–5718, <https://doi.org/10.5194/hess-29-5695-2025>, 2025.
- 614 Beniston, M., Stephenson, D. B., Christensen, O. B., Ferro, C. A. T., Frei, C., Goyette, S., Halsnaes, K., Holt,
615 T., Jylhä, K., Koffi, B., Palutikof, J., Schöll, R., Semmler, T., and Woth, K.: Future extreme events in European
616 climate: an exploration of regional climate model projections, *Clim. Change*, 81, 71–95,
617 <https://doi.org/10.1007/s10584-006-9226-z>, 2007.
- 618 Beria, H., Larsen, J. R., Michelon, A., Ceperley, N. C., and Schaeffli, B.: HydroMix v1.0: a new Bayesian
619 mixing framework for attributing uncertain hydrological sources, *Geosci. Model Dev.*, 13, 2433–2450,
620 <https://doi.org/10.5194/gmd-13-2433-2020>, 2020.
- 621 Carrer, M., Dibona, R., Prendin, A. L., and Brunetti, M.: Recent waning snowpack in the Alps is unprecedented
622 in the last six centuries, *Nat. Clim. Chang.*, 13, 155–160, <https://doi.org/10.1038/s41558-022-01575-3>, 2023.
- 623 Chen, J., Brissette, F. P., Chaumont, D., and Braun, M.: Finding appropriate bias correction methods in
624 downscaling precipitation for hydrologic impact studies over North America, *Water Resour. Res.*, 49, 4187–
625 4205, <https://doi.org/10.1002/wrcr.20331>, 2013.
- 626 Dall’Amico, M., Tasin, S., Di Paolo, F., Brian, M., Leoni, P., Tornatore, F., Formetta, G., Wani, J. M., Rigon,
627 R., and Roati, G.: 30-years (1991-2021) Snow Water Equivalent Dataset in the Po River District, Italy, *Sci.*
628 *Data*, 12, 374, <https://doi.org/10.1038/s41597-025-04633-5>, 2025.
- 629 Estermann, R., Rajczak, J., Velasquez, P., Lorenz, R., and Schär, C.: Projections of Heavy Precipitation
630 Characteristics Over the Greater Alpine Region Using a Kilometer–Scale Climate Model Ensemble, *Journal of*
631 *Geophysical Research: Atmospheres*, 130, e2024JD040901, <https://doi.org/10.1029/2024JD040901>, 2025.
- 632 Eum, H.-I., Gupta, A., and Dibike, Y.: Effects of univariate and multivariate statistical downscaling methods on
633 climatic and hydrologic indicators for Alberta, Canada, *J. Hydrol. (Amst.)*, 588, 125065,
634 <https://doi.org/https://doi.org/10.1016/j.jhydrol.2020.125065>, 2020.
- 635 François, B., Vrac, M., Cannon, A. J., Robin, Y., and Allard, D.: Multivariate bias corrections of climate
636 simulations: which benefits for which losses?, *Earth Syst. Dynam.*, 11, 537–562, <https://doi.org/10.5194/esd-11-537-2020>, 2020.
- 638 Frei, P., Kotlarski, S., Liniger, M. A., and Schär, C.: Future snowfall in the Alps: projections based on the
639 EURO-CORDEX regional climate models, *Cryosphere*, 12, 1–24, <https://doi.org/10.5194/tc-12-1-2018>, 2018.
- 640 Hakala, K., Addor, N., and Seibert, J.: Hydrological Modeling to Evaluate Climate Model Simulations and Their
641 Bias Correction, *J. Hydrometeorol.*, 19, 1321–1337, <https://doi.org/10.1175/JHM-D-17-0189.1>, 2018.
- 642 van Hamel, A. and Brunner, M. I.: Trends and Drivers of Water Temperature Extremes in Mountain Rivers,
643 *Water Resour. Res.*, 60, e2024WR037518, <https://doi.org/10.1029/2024WR037518>, 2024.
- 644 Harpold, A. A., Kaplan, M. L., Klos, P. Z., Link, T., McNamara, J. P., Rajagopal, S., Schumer, R., and Steele,
645 C. M.: Rain or snow: hydrologic processes, observations, prediction, and research needs, *Hydrol. Earth Syst.*
646 *Sci.*, 21, 1–22, <https://doi.org/10.5194/hess-21-1-2017>, 2017.
- 647 Jenicek, M., Seibert, J., Zappa, M., Staudinger, M., and Jonas, T.: Importance of maximum snow accumulation
648 for summer low flows in humid catchments, *Hydrol. Earth Syst. Sci.*, 20, 859–874, <https://doi.org/10.5194/hess-20-859-2016>, 2016.
- 650 Klein, G., Vitasse, Y., Rixen, C., Marty, C., and Rebetez, M.: Shorter snow cover duration since 1970 in the
651 Swiss Alps due to earlier snowmelt more than to later snow onset, *Clim. Change*, 139, 637–649,
652 <https://doi.org/10.1007/s10584-016-1806-y>, 2016.
- 653 Kotlarski, S., Gobiet, A., Morin, S., Olefs, M., Rajczak, J., and Samacoïts, R.: 21st Century alpine climate
654 change, *Clim. Dyn.*, 60, 65–86, <https://doi.org/10.1007/s00382-022-06303-3>, 2023.



- 655 Lüthi, S., Ban, N., Kotlarski, S., Steger, C. R., Jonas, T., and Schär, C.: Projections of Alpine Snow-Cover in a
656 High-Resolution Climate Simulation, <https://doi.org/10.3390/atmos10080463>, 2019.
- 657 Magnusson, J., Gustafsson, D., Hüsler, F., and Jonas, T.: Assimilation of point SWE data into a distributed snow
658 cover model comparing two contrasting methods, *Water Resour. Res.*, 50, 7816–7835,
659 <https://doi.org/https://doi.org/10.1002/2014WR015302>, 2014.
- 660 Marke, T., Strasser, U., Hanzer, F., Stötter, J., Wilcke, R. A. I., and Gobiet, A.: Scenarios of Future Snow
661 Conditions in Styria (Austrian Alps), *J. Hydrometeorol.*, 16, 261–277, <https://doi.org/10.1175/JHM-D-14->
662 0035.1, 2015.
- 663 Marty, C., Schlögl, S., Bavay, M., and Lehning, M.: How much can we save? Impact of different emission
664 scenarios on future snow cover in the Alps, *Cryosphere*, 11, 517–529, <https://doi.org/10.5194/tc-11-517-2017>,
665 2017a.
- 666 Marty, C., Tilg, A.-M., and Jonas, T.: Recent Evidence of Large-Scale Receding Snow Water Equivalents in the
667 European Alps, *J. Hydrometeorol.*, 18, 1021–1031, <https://doi.org/10.1175/jhm-d-16-0188.1>, 2017b.
- 668 Marty, C., Michel, A., Jonas, T., Steijn, C., Muelchi, R., and Kotlarski, S.: SPASS – new gridded climatological
669 snow datasets for Switzerland: potential and limitations, *Cryosphere*, 19, 4391–4407, <https://doi.org/10.5194/tc->
670 19-4391-2025, 2025.
- 671 Matiu, M. and Hanzer, F.: Bias adjustment and downscaling of snow cover fraction projections from regional
672 climate models using remote sensing for the European Alps, *Hydrol. Earth Syst. Sci.*, 26, 3037–3054,
673 <https://doi.org/10.5194/hess-26-3037-2022>, 2022.
- 674 Matiu, M., Crespi, A., Bertoldi, G., Carmagnola, C. M., Marty, C., Morin, S., Schöner, W., Cat Berro, D.,
675 Chiogna, G., De Gregorio, L., Kotlarski, S., Majone, B., Resch, G., Terzago, S., Valt, M., Beozzo, W.,
676 Cianfarra, P., Gouttevin, I., Marcolini, G., Notarnicola, C., Petitta, M., Scherrer, S. C., Strasser, U., Winkler, M.,
677 Zebisch, M., Cicogna, A., Cremonini, R., Debernardi, A., Faletto, M., Gaddo, M., Giovannini, L., Mercalli, L.,
678 Soubeyroux, J.-M., Sušnik, A., Trenti, A., Urbani, S., and Weilguni, V.: Observed snow depth trends in the
679 European Alps: 1971 to 2019, *Cryosphere*, 15, 1343–1382, <https://doi.org/10.5194/tc-15-1343-2021>, 2021.
- 680 Matiu, M., Napoli, A., Kotlarski, S., Zardi, D., Bellin, A., and Majone, B.: Elevation-dependent biases of raw
681 and bias-adjusted EURO-CORDEX regional climate models in the European Alps, *Clim. Dyn.*,
682 <https://doi.org/10.1007/s00382-024-07376-y>, 2024.
- 683 Mayer, S., Hendrick, M., Michel, A., Richter, B., Schweizer, J., Wernli, H., and van Herwijnen, A.: Impact of
684 climate change on snow avalanche activity in the Swiss Alps, *Cryosphere*, 18, 5495–5517,
685 <https://doi.org/10.5194/tc-18-5495-2024>, 2024.
- 686 MeteoSwiss: Documentation of MeteoSwiss Grid-Data Products: Daily Precipitation (final analysis): RhiresD,
687 Zürich, 4 pp., 2016.
- 688 MeteoSwiss: Documentation of MeteoSwiss Grid-Data Products: Daily mean, minimum and maximum
689 temperature, Zürich, 4 pp., 2017.
- 690 MeteoSwiss and Zurich, E.: Climate CH2025 - Scientific Report, Zurich,
691 <https://doi.org/10.18751/climate/scenarios/ch2025/sr/1.0/>, 2025.
- 692 Meyer, J., Kohn, I., Stahl, K., Hakala, K., Seibert, J., and Cannon, A. J.: Effects of univariate and multivariate
693 bias correction on hydrological impact projections in alpine catchments, *Hydrol. Earth Syst. Sci.*, 23, 1339–
694 1354, <https://doi.org/10.5194/hess-23-1339-2019>, 2019.
- 695 Michel, A., Brauchli, T., Lehning, M., Schaeffli, B., and Huwald, H.: Stream temperature and discharge
696 evolution in Switzerland over the last 50 years: annual and seasonal behaviour, *Hydrol. Earth Syst. Sci.*, 24,
697 115–142, <https://doi.org/10.5194/hess-24-115-2020>, 2020.
- 698 Michel, A., Sharma, V., Lehning, M., and Huwald, H.: Climate change scenarios at hourly time-step over
699 Switzerland from an enhanced temporal downscaling approach, *International Journal of Climatology*, 41, 3503–
700 3522, <https://doi.org/10.1002/joc.7032>, 2021.



- 701 Michel, A., Aschauer, J., Jonas, T., Gubler, S., Kotlarski, S., and Marty, C.: SnowQM 1.0: a fast R package for
702 bias-correcting spatial fields of snow water equivalent using quantile mapping, *Geosci. Model Dev.*, 17, 8969–
703 8988, <https://doi.org/10.5194/gmd-17-8969-2024>, 2024.
- 704 Morin, S., Samacoïts, R., François, H., Carmagnola, C. M., Abegg, B., Demiroglu, O. C., Pons, M.,
705 Soubeyroux, J.-M., Lafaysse, M., Franklin, S., Griffiths, G., Kite, D., Hoppler, A. A., George, E., Buontempo,
706 C., Almond, S., Dubois, G., and Cauchy, A.: Pan-European meteorological and snow indicators of climate
707 change impact on ski tourism, *Clim. Serv.*, 22, 100215,
708 <https://doi.org/https://doi.org/10.1016/j.cliser.2021.100215>, 2021.
- 709 Mott, R., Winstral, A., Cluzet, B., Helbig, N., Magnusson, J., Mazzotti, G., Quéno, L., Schirmer, M., Webster,
710 C., and Jonas, T.: Operational snow-hydrological modeling for Switzerland, *Front. Earth Sci. (Lausanne)*,
711 Volume 11, <https://doi.org/10.3389/feart.2023.1228158>, 2023.
- 712 Obuchowicz, C., Poussin, C., and Giuliani, G.: Change in observed long-term greening across Switzerland –
713 evidence from a three decades NDVI time-series and its relationship with climate and land cover factors, *Big
714 Earth Data*, 1–32, <https://doi.org/10.1080/20964471.2023.2268322>, 2023.
- 715 Olefs, M., Koch, R., Schöner, W., and Marke, T.: Changes in Snow Depth, Snow Cover Duration, and Potential
716 Snowmaking Conditions in Austria, 1961–2020—A Model Based Approach,
717 <https://doi.org/10.3390/atmos11121330>, 2020.
- 718 Peßenteiner, S., Hohmann, C., Kirchengast, G., and Schöner, W.: High-resolution climate datasets in
719 hydrological impact studies: Assessing their value in alpine and pre-alpine catchments in southeastern Austria,
720 *J. Hydrol. Reg. Stud.*, 38, 100962, <https://doi.org/10.1016/j.ejrh.2021.100962>, 2021.
- 721 Ranzi, R., Colosio, P., and Galeati, G.: Climatology of snow depth and water equivalent measurements in the
722 Italian Alps (1967–2020), *Hydrol. Earth Syst. Sci.*, 28, 2555–2578, <https://doi.org/10.5194/hess-28-2555-2024>,
723 2024.
- 724 Rätý, O., Räisänen, J., Bosshard, T., and Donnelly, C.: Intercomparison of Univariate and Joint Bias Correction
725 Methods in Changing Climate From a Hydrological Perspective, <https://doi.org/10.3390/cli6020033>, 2018.
- 726 Rottler, E., Storebakken, B., Warscher, M., Hanzer, F., Bertazza, E., and Strasser, U.: Assessment of snow
727 model uncertainty in relation to the effect of a 1 °C warming using the snow modelling framework
728 openAMUNDSEN, *Cryosphere*, 20, 2351–2373, <https://doi.org/10.5194/tc-20-2351-2026>, 2026.
- 729 Schaeffli, B.: Projecting hydropower production under future climates: a guide for decision-makers and modelers
730 to interpret and design climate change impact assessments, *Wiley Interdisciplinary Reviews: Water*, 2, 271–289,
731 <https://doi.org/10.1002/wat2.1083>, 2015.
- 732 Schmucki, E., Marty, C., Fierz, C., and Lehning, M.: Simulations of 21st century snow response to climate
733 change in Switzerland from a set of RCMs, *International Journal of Climatology*, 35, 3262–3273,
734 <https://doi.org/10.1002/joc.4205>, 2015.
- 735 Schmucki, E., Marty, C., Fierz, C., Weingartner, R., and Lehning, M.: Impact of climate change in Switzerland
736 on socioeconomic snow indices, *Theor. Appl. Climatol.*, 127, 875–889, <https://doi.org/10.1007/s00704-015-1676-7>, 2017.
- 738 Schöner, W., Koch, R., Matulla, C., Marty, C., and Tilg, A.-M.: Spatiotemporal patterns of snow depth within
739 the Swiss-Austrian Alps for the past half century (1961 to 2012) and linkages to climate change, *International
740 Journal of Climatology*, 39, 1589–1603, <https://doi.org/10.1002/joc.5902>, 2019.
- 741 Serquet, G., Marty, C., Dulex, J.-P., and Rebetez, M.: Seasonal trends and temperature dependence of the
742 snowfall/precipitation-day ratio in Switzerland, *Geophys. Res. Lett.*, 38,
743 <https://doi.org/https://doi.org/10.1029/2011GL046976>, 2011.
- 744 Verfaillie, D., Lafaysse, M., Déqué, M., Eckert, N., Lejeune, Y., and Morin, S.: Multi-component ensembles of
745 future meteorological and natural snow conditions for 1500 m altitude in the Chartreuse mountain range,
746 Northern French Alps, *Cryosphere*, 12, 1249–1271, <https://doi.org/10.5194/tc-12-1249-2018>, 2018.



- 747 Vorkauf, M., Marty, C., Kahmen, A., and Hiltbrunner, E.: Past and future snowmelt trends in the Swiss Alps:
748 the role of temperature and snowpack, *Clim. Change*, 165, 1–19, <https://doi.org/10.1007/s10584-021-03027-x>,
749 2021.
- 750 Willibald, F., Kotlarski, S., Ebner, P. P., Bavay, M., Marty, C., Trentini, F. V, Ludwig, R., and Grêt-Regamey,
751 A.: Vulnerability of ski tourism towards internal climate variability and climate change in the Swiss Alps,
752 *Science of The Total Environment*, 784, 147054, <https://doi.org/https://doi.org/10.1016/j.scitotenv.2021.147054>,
753 2021.
- 754 Wüest, R. O., Bergamini, A., Bollmann, K., and Baltensweiler, A.: LiDAR data as a proxy for light availability
755 improve distribution modelling of woody species, *For. Ecol. Manage.*, 456, 117644,
756 <https://doi.org/https://doi.org/10.1016/j.foreco.2019.117644>, 2020.
- 757